RESEARCH ARTICLE

Half antiperovskites VII – DFT modelling of shandites that are isoelectronic to Co$_3$Sn$_2$S$_2$

Clara Marx,[a] Jan Endriss,[a] Maxi Klopfer,[a] Werner Reichel,[a] Christian Strakos,[a] and Richard Weihrich*[a]

Dedicated to Prof. Dr. R. Dronskowski on the occasion of his birthday

Our discovery of half metal ferromagnetic (HFM) properties on shandite type Co$_3$Sn$_2$S$_2$=Sn$_2$Co$_3$S$_2$ about 20 years ago by DFT calculations opened the gate for fascinating discoveries like giant anomalous Hall effect and Weyl semimetal characteristics. Thereby, interest arose on electronic and magnetic structure effects upon substitution of M=Co and A=Sn sites in and between Co Kagomé layers. Non isoelectronic substitution to A=In or M=Ni causes a decay of magnetic properties to semiconducting diamagnetic InSnCo$_3$S$_2$ or paramagnetic semi metal Ni$_3$Sn$_2$S$_2$. The present study addresses simultanious substitutions on both A and M sites to novel isoelectronic compounds of Co$_3$Sn$_2$S$_2$. Therefore, DFT calculations were performed on model structures MM′$_2$AA′X$_2$ (M=Fe, Co, Ni; A=In, Sn, Sb; X=S). By the given approach, target compositions are identified that are interesting for future investigations and discoveries.

Introduction

Shandite is the mineral Pb$_2$Ni$_3$S$_2$, discovered in 1949 by Paul Ramdohr on a sample of the mineral heazlewoodit, Ni$_3$S$_2$.[1] He could synthesize the compound and correctly proposed its trigonal symmetry. It was confirmed by Peacock et al. (space group: R$\bar{3}$m, lattice parameters a=5.565 Å, α=60.2°, V=122.59 Å^3, Z=1).[2] In subsequent decades isotypic compounds A$_2$M$_3$X$_2$ were prepared by chemical synthesis with main group A=In, Sn, Tl, Pb, transition group metals M=Co, Ni, Rh, Pd, non-metals X=S, Se).[3–9] In search for interesting properties ferromagnetism was proposed for shandite and Pb$_2$Ni$_3$Se$_2$[3] but in subsequent studies[4–5] only Pauli paramagnetism was found for shandites. Hillers results were attributed to Ni impurities.

Fascinating magnetism was however found for the cobalt-shandite Sn$_2$Co$_3$S$_2$. It was first prepared by Zabel and Range[6] in Regensburg and re-investigated there starting in 1998 with new insights in crystal and electronic structures, and properties.[7–9] Its structure was refined and Sn$_2$Co$_3$S$_2$ was discovered as S=$\frac{1}{2}$ half metal ferromagnet (HFM) from DFT calculations.[7–9] The kink observed in conductivity versus temperature curves by Natarajan et al. was attributed to a transition from a Pauli paramagnet to a band ferromagnet below T$_C$=−97 °C (176 K).

A simple description of the crystal structure of shandites A$_2$M$_3$X$_2$ was developed from the "role" of the A, M, and X atoms.[10–12] In shandites, monoclinic and cubic parkerites Bi$_2$Ni$_3$S$_2$ and Bi$_2$Pd$_3$S$_2$ the main group metals A form a simple primitive structure centered by X. The M atoms are found in tetragonal bipamieds A$_4$X$_2$ similar to antiperovskites AM$_3$X like MgNi$_3$C. As in shandites and parkerites only half of M sites are occuped, they were called "half antiperovskites" AM$_{3/2}$X=A$_2$M$_3$X$_2$. Interestingly, a similar structure relation was described by Hoppe to oxostannates like K$_2$Sn$_2$O$_3$=KSnO$_{3/2}$. Similar to Ti–O–Ti bonds in perovskites the M atoms in antiperovskites are linearly coordinated by S–M–S bonds in covalent [M$_3$S$_2$] networks as mentioned by the description A$_2$[M$_3$X$_2$].

A "chemical" understanding of electronic structure and HFM magnetism in Sn$_2$Co$_3$S$_2$ was derived from crystal structure and electron counting.[7–9] HFM compounds are metals for one spin channel, but semi-conductors for the other. Respective Heusler alloys, CrO$_2$ (Cr^{4+}, 3d^2), or CoS$_2$ (low-spin Co^{2+}, d^7, S=$\frac{1}{2}$) are band ferromagnets, but their magnetism can be understood from ionic spin states. For Sn$_2$Co$_3$S$_2$ band structures predicted an I$_A$-type HFM with S=$\frac{1}{2}$.[7–9] It is understood by Co(0)-3d^9-states that interact within face sharing Sn$_4$S$_2$ polyhedra. This causes the formation of a band gap between bands no. 23 and 24. In Sn$_2$Co$_3$S$_2$ (47 valence electrons, VE) the conduction band (CB) is occupied by only 1 electron that is responsible for its magnetism. Schnelle et al. and other groups confirmed the predicted HFM state experimentally. Sn$_2$Co$_3$S$_2$ turned out as highly anisotropic HFM that is magnetized perpendicular to Co kagomé nets.[13–16]

Substitution of A=Sn atoms by In cause a change in electron count and magnetism. InSnCo$_3$S$_2$ (46 VE) has one electron less than Sn$_2$Co$_3$S$_2$. The fermi energy E$_F$ is shift into the gap. InSnCo$_3$S$_2$ is a low gap semiconductor and thermoelectric material.[7–9] Additionally, the electronic structure turned out

[a] C. Marx, J. Endriss, M. Klopfer, W. Reichel, C. Strakos, Prof. Dr. R. Weihrich
Institute for Materials Resource Management, University of Augsburg,
Am Technologiezentrum 8, D-86159 Augsburg, Germany
E-mail: richard.weihrich@uni-a.de

sensitive to occupation of A-In, Sn between and in Co kagomé layer. Ordering of In and Sn modulates the band gap.[17–21]

Substitution on $M=$Co sites $Sn_2Co_3S_2$ by Ni increases the number of electrons towards $Sn_2Ni_3S_2$ (50 VE). In solid solutions $Sn_2Co_{3-x}Ni_xS_2$ magnetism decays.[13] It is understood by filling the d-bands towards Ni(0)-3d[10[7,22]] compared to Co(0)-3d[9].[9] To the contrary, substitutions of $M=$Co by Fe, Mn, Cr[23] reduce the number of electrons. According to DFT calculations the respective compounds are predicted as HFM materials. However, they were not prepared to date except $Sn_2FeCo_2S_2$ that was found isoelectronic to $InSnCo_3S_2$ and semiconducting, too.[24]

Recently, the electronic structure for $Sn_2Co_3S_2$ was enriched by outstanding discoveries on 2D magnetism and topological properties.[25–27] Its giant anomalous Hall effect (GAHE) was intrinsically related to Weyl semimetal behavior. Now, focus turned on valence bands no. 24 and 25 that cross at two k-points. Spin-orbit coupling opens gaps at the respective points at E_F characterized as Weyl points. Accordingly, $Sn_2Co_3S_2$ was classified as magnetic Weyl-semimetal with large anomalous hall conductivity (AHC) and a huge anomalous hall angle (AHA). The electronic topology of the cobalt-shandite was estimated as a guide to the realization of strong AHE in magnetic and topological semimetals. Researchers started to exploit further properties of $Sn_2Co_3S_2=Co_3Sn_2S_2$ including zero field Nernst effect, thermoelectric and magnetocaloric properties, as well as critical and Skyrmion behavior (see e.g.[28–35]).

The discoveries shed light into the valence band region of $Sn_2Co_3S_2$: all fascinating properties like half-metal ferromagnetism, Weyl and topological properties of $Sn_2Co_3S_2$, and semiconductivity of $InSn_2Co_3S_2$ depend on only 3 bands, i.e. no 23, 24, and 25. Chemically, one can see these three bands as bonding, non-bonding, and antibonding states of interactions of e_g-orbitals (Co-3d[9]) within Co Kagomé layers.[9] The position and topology of these bands is determined by Co–Co, but also by Co–S and Co–Sn-bands within Sn_4S_2 polyhedra as studied by the electron localization function (ELF).[36,37] According to first results on partial M site substitution by Ni[38] simultaneous substitution of A site atoms directs a way to tune band topology.

20 years ago, our DFT predictions initiated fascinating discoveries on $Sn_2Co_3S_2$. The present study focusses on DFT modeling of multinary shandites $AA'MM'_2S_2$ ($M=$Fe, Co, Ni, $A=$In, Sn, Sb) that are isoelectronic to $Sn_2Co_3S_2$. First, their crystal structures are discussed, then electronic structures. The aim is to identify again interesting target systems for future studies.

structures. Metric relations of the trigonal cell in primitive rhombohedral (*rh*, Z=1) and hexagonal (*hex*, Z=3) setting and the monoclinic cell are illustrated in Figure 1. For $Sn_2Co_3S_2$ hexagonal ($a_{hex}=5.368(1)$ Å, $c_{hex}=13.177(1)$ Å, $V_{hex}=328.8$ Å³, Z=3), trigonal ($a_{rh}=5.376$ Å, $\alpha_{rh}=59.91$ Å, $V_{rh}=109,4$ Å³, Z=1),[6–8] and monoclinic ($a_m=9.315$ Å, $b_m=a_{rh}$, $c_m=a_{hex}$; ß=125.36°) unit cells are shown. By transformation of *B2/m* setting to *C2/m* the axis b_m becomes c_m and *vice versa*. Indeed, shandites with $A=$In differ in trigonal distortion, with significant longer c_{hex}-axis (13.6 Å) and smaller angle $\alpha_{rh}=57.9°$ as shown in Figure 1.[6,10] Table 1 presents the related atomic coordinates for the trigonal and monoclin cell for $Sn_2Co_3S_2$.
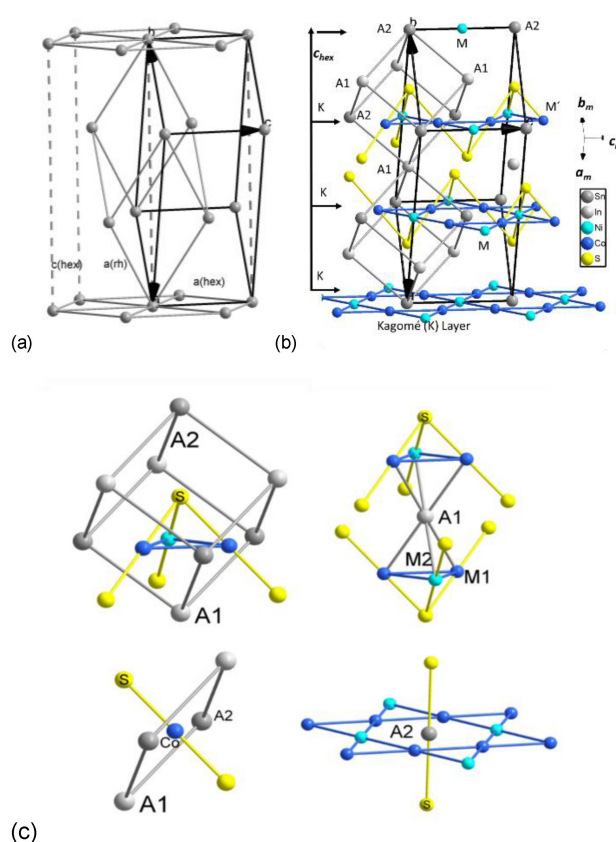

Figure 1. (a) metric relations of trigonal rhombohedral (*rh*), hexagonal (*hex*), and monoclinic cell, (b) Model structure of $InSnNiCo_2S_2$ (monoclinic cell), (c) atomic coordination spheres for *A1*, *A2*, *M*, and S sites. (main group metal $A=$In, Sn, Sb; transition group metal $M=$Co, Ni, Rh, Pd; chalcogen $X=$S, Se Te).

Results and Discussion

The AA'MM'₂S₂ structure model

In 1976 Michelet et al presented the structure of $Sn_2Ni_3S_2$ in a monoclinic cell of space group *C2/m* (*B2/m* setting, Z=2).[3] Zabel transformed it to the trigonal shandite type cell (*R3̄m*).[4] He related the deviation from cubic metrics to trigonal distortion and concluded that all shandites crystallize in isotypic

Table 1. Atomic coordinates for $Sn_2Co_3S_2$, trigonal and monoclinic cells.

	Trigonal prim. $R\bar{3}m$	Hexagonal $R\bar{3}m$	Monoclinic $B2/m$
A1	1a (0,0,0)	3a (0,0,0)	2a (0,0,0)
A2	1b ($^1/_2$,$^1/_2$,$^1/_2$)	1b (0,0,$^1/_2$)	2c ($^1/_2$,$^1/_2$,0)
M1	3d ($^1/_2$,$^1/_2$,0,)	9d ($^1/_2$,0,$^1/_2$)	2b (0,0,$^1/_2$)
M2			4f ($^1/_4$,$^1/_2$,$^1/_4$)
X=S	2c (z,z,z=0.2828(1))	6c (0,0,z)	4i ($^1/_2$−z, $^1/_2$+z,0)

Table 2. Compositions and calculated cell parameters from DFT-PBE-D3 structure optimizations.

	SG	a/Å	b/Å	c/Å		γ/°	V/Å³
$Sn_2Co_3S_2$	$B2/m$	9.291	5.349	5.300		125.88	213.44
$Sn_2Co_3S_2$	$R\bar{3}m$	5.300	5.348	13.159		59.41	106.72
$InSbCo_3S_2$	$B2/m$	9.499	5.421	5.231		127.63	213.35
$InSbCo_3S_2$	$R\bar{3}m$	5.238	5.424	13.507		57.75	107.00
$SbInCo_3S_2$	$B2/m$	9.072	5.281	5.406		123.64	215.61
$SbInCo_3S_2$	$R\bar{3}m$	5.416	5.284	12.777		61.66	108.18
$InSnCo_2NiS_2$	$B2/m$	9.588	5.470	5.271		127.79	217.75
$SnInCo_2NiS_2$	$B2/m$	9.311	5.412	5.340		125.56	218.89
$In_2CoNi_2S_2$	$B2/m$	9.646	5.452	5.330		127.37	222.78
$InSnFeNi_2S_2$	$B2/m$	9.657	5.440	5.278		127.60	219.72
$SnInFeNi_2S_2$	$B2/m$		9.487	5.315	5.404	125.93	220.64
$SnSbFeCo_2S_2$	$B2/m$		9.269	5.337	5.262	125.90	210.90
$SbSnFeCo_2S_2$	$B2/m$		9.121	5.269	5.354	124.39	212.33

In the trigonal cells Co atoms occupy $9d$ ($\frac{1}{2}$,0,0) sites forming kagomé layers. Contrary Laves phases the atomic distances $d_{Co\text{-}Co} = 2.68\,\text{Å} = a_{hex}/2$ therein are longer than in the respective element ($d_{Co\text{-}Co} = 2.5\,\text{Å}$), indicative for weak Co–Co interactions. Two main group metal sites $A = Sn$ are found. $A1$ site atoms on $3a$ (0,0,0) interlink Co_3 triangles between layers. The $A2$ site on $3b$ (0,0,$\frac{1}{2}$) is found in M_6 hexagons of the layers. Metal Co–Sn bonds are suggested strong and determined by relations $d_{Sn1\text{-}Co} = a_{rh}/2$ and $d_{Sn2\text{-}Co} = a_{hex}/2 = d_{Co\text{-}Co}$. As shown for ordered structures of $InSnCo_3S_2$, $A2$ site atoms determine A-M and M–M distances in the layers, $A1$ site atoms interlayer-distances. Co layers are spaced by $c_{hex}/3 = 13.18/3\,\text{Å} = 4.4\,\text{Å}$ with $A1$ and S atoms on top and below Co_3 triangles. In the HAP structure relation the Co atoms are found on faces of the $A = Sn$ substructure centered by S. In case of $Sn_2Co_3S_2$ the Co atoms occupy half of tetragonal bipyramid sites Sn_4S_2. The $CoSn_4S_2$ polyhedral are interlinked by faces within the layers and by Sn1 atoms between the layers. Therein short distances $d_{Co\text{-}S} = 2.18\,\text{Å}$ and linear S–M–S arrangements led to conclusion on covalent $[M_3S_2]$ networks.

Substitution of $A1$ and $A2$ site metals can be modeled in ordered structure of the trigonal cell as done for $InSnCo_3S_2$. To model structures for compositions $AA'MM'_2S_2$ with partial A and M site substitution, the monoclinic cell ($Z = 2$) is subsequently applied. M sites split into $2b$ and $4f$. This allows to describe ordered $AA'MM'_2S_2$ structures, e.g. for $InSnNiCo_2S_2$.

Crystal structure calculations

Possible compositions and results for $AA'MM'_2S_2$ compounds with $A = In$, Sn, Sb, $M = Fe$, Co, Ni that are isoelectronic to $Sn_2Co_3S_2$ (47 valence electrons, VE) were summarized in Table 3. By simultaneous substitution of A and M sites number of electrons are balanced when electrons are added on one of the A or M sites and subtracted from the other. As an example, one Co atom is replaced by Ni (one electron more) in $Sn_2Co_3S_2$ and one Sn atom by In (one electron less) to obtain the composition $InSnNiCo_2S_2$. DFT optimizations were performed with ordered model structures in the monoclinic cell of $B2/m$ setting.

Table 3. Compositions and calculated cell parameters form DFT-PBE-D3 structure optimizations ($B2/m$ cell).

	a/Å	b/Å	c/Å	γ/°	V/Å³
$Sn_2Co_3S_2$	9.181	5.287	5.244	125.82	206.39
$SnInCo_2NiS_2$	9.186	5.350	5.280	125.47	211.37
$InSnCo_2NiS_2$	9.426	5.399	5.216	127.58	210.36
$In_2CoNi_2S_2$	9.503	5.375	5.280	127.25	214.70
$InSnFeNi_2S_2$	9.525	5.379	5.216	127.47	212.11
$SnInFeNi_2S_2$	9.373	5.255	5.346	125.91	213.26
$SnSbFeCo_2S_2$	9.171	5.283	5.190	125.93	203.59
$SbSnFeCo_2S_2$	9.027	5.215	5.290	124.43	205.40
$SbInCo_3S_2$	8.983	5.225	5.333	123.84	207.88
$InSbCo_3S_2$	9.368	5.347	5.168	127.57	205.18

$Sn_2Co_3S_2$, $InSbCo_3S_2$, and $SbInCo_3S_2$ were additionally calculated with trigonal cells. Here, and in all subsequent compositions A site occupation is described by the order of the atoms $A1\ A2MM_2X_2$ with $A1$ (between Co layers) and $A2$ (in the layers).

The present calculations are based on models that imply $A1$–$A2$ and M–M'-site ordering. In case of $InSnCo_3S_2$ the ordered structures turned out as good approximants for understanding crystal and electronic structures of the experimentally obtained samples. Therein, Sn prefers the $A2$ sites in the kagomé layers and In the $A1$ sites between them. Substitutions $M = Ni$, Co, Fe in shandites are experimentally known. Due to close atomic radii models with M site ordering for $M = Fe$, Co, Ni should serve as suitable approximants for future experimental studies, too. This also accounts for predicted structures with $A = Sb$, that are not known to date, but turn out as interesting candidates.

Table 2 summarizes results from full structural relaxations with the PBE functional. For $Sn_2Co_3S_2$ the present PBE calculations predict a volume of 107 Å³, close experimental values at −120 °C, and 103.2 Å³ when dispersion interactions are accounted for by PBE + D3 parametrization (Table 3). This trend is seen systematically for all studied compositions. Cell volumes from PBE + D3 calculations are approx. 2.5 % smaller than from PBE calculations. One must conclude on contributions of dispersion interactions to bonding in shandites. A very simple isoelectronic substitution is found for $InSbCo_3S_2$ and $SbInCo_3S_2$ where In (Z = 49) has one electron less and Sb (Z =

51) one electron more than Sn (Z = 50). The calculated trigonal cells show only slightly larger volumes than $Sn_2Co_3S_2$. The hexagonal c axis is much longer when $A1 = In$, but shorter for $A1 = Sb$. The influence of the $A2$ site atom is seen from a_{hex} (= c_m) that becomes longer for $A2 = In$ (5.42 Å) than for $A2 = Sb$ (5.30 Å). Similar trends are known for $InSnCo_3S_2$.[18,19]

In the monoclinic cell setting the longer interlayer distances are reflected by larger values for a_m cell parameters, as seen for $InSnCo_2NiS_2$ and $SnInCo_2NiS_2$. Again, In on interlayer $A1$ sites causes longer interlayer distances than $A1 = Sn$. As known from $InSnCo_3S_2$ the exchange of In and Sn on $A1$ and $A2$ sites causes similar cell volumes. The increase in cell volume by 5 Å³ compared to $Sn_2Co_3S_2$ is attributed to Ni. On the other hand, In on $A2$ sites causes similar bonding distances in kagomé layers as found for isoelectronic $In_2Ni_2CoS_2$. Here, the second Sn atom is replaced by In and an additional Co atom by Ni that causes again an increase in cell volume compared to $Sn_2Co_3S_2$.

Isoelectronic compounds are obtained when one Co atom is replaced by Fe instead of Sn by In. Indeed, the cell volume calculated for $SnInFeNi_2S_2$ is in the same range obtained for $SnInCo_2NiS_2$. The insertion of Sb instead of Sn is predicted to cause a decrease in cell volume in $SnSbFeCo_2S_2$. Interestingly, the Sb containing models are predicted with cell volumes close to $Sn_2Co_3S_2$. For so far, no shandites with $A = Sb$ were prepared. There seems to be a limit in the stability of the shandite structure where pyrite related 1:1:1 compositions become more stable. To date in the phase diagram Co–Sb–S only CoSbS, but no "$Sb_2Co_3S_2$" is known. However, the coexistence of both stoichiometries is known for NiBiSe and $Bi_2Ni_3Se_2$.[39]

The non-trivial relation of cell volumes and compositions is illustrated in Figure 2 from calculations on the equations-of-state (EOS). Here, the results from PBE + D3-calculations are shown. One can state that a huge range of differing cell volumes from 100 Å³ to 107 Å³ can be obtained for isoelectronic compositions. From the comparison of $In_2CoNi_2S_2$, $InSbCo_3S_2$, and $SnSbFeCo_2S$ one con conclude on effects of individual atoms on the cell volume. It is the composition and the specific site occupation that causes the cell volume. As mentioned before, electronic structure and magnetism of $Sn_2Co_3S_2$ is known to be sensiti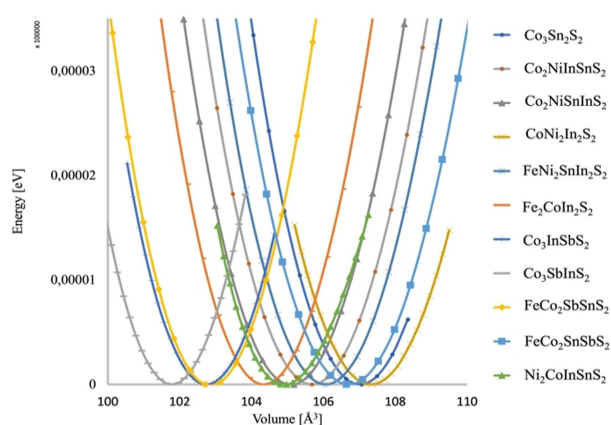ve to the cell volume and the band structure of $InSnCo_3S_2$ is manipulated by A site occupation. Substitution effects might thus be interesting to stabilize or to tune topological and magnetic states in $Sn_2Co_3S_2$.

Electronic structure

Fundamental concepts of the electronic structure of $Sn_2Co_3S_2$ are introduced in Figure 3 for further discussions. First, the orbital order in shandites is presented as obtained from analysis of the atomic orbital projected density of states (DOS, see[7,9] and Figure 4a). Following the structure and composition, it is simply obtained from the atomic orbitals: four orbital states are received from two S-3s and 2 Sn-5s orbitals in $Sn_2Co_3S_2$. Next, six orbitals are introduced by sulfur 3p orbitals of two S atoms. Two occupied S-3s², two Sn-5s², and six S-3p⁶ orbitals sum up to 10 bands and 20 electrons per FU. Co-3d⁹ states from 3 Co-atoms sum up to 15 d-orbitals and 27 electrons. Together with the S- and Sn-states 47 valence electrons and 25 bands are obtained. In a simple ionic view, the Sn-5p states remain empty in $Sn_2Co_3S_2$. However, they contribute to metallic bonding.[36,37]

For Co(0)-3d⁹-configurations four 3d orbitals are fully occupied for each Co atom resulting in 12 bands per formula unit $Sn_2Co_3S_2$. Adding 10 bands and 20 electrons from the "Sn_2S_2" partial structure we receive $10 + 12 = 22$ VB valence bands that are fully occupied by $20 + 24 = 44$ valence electrons. In the Co-3d⁹ state each Co-atom has one half occupied $(d_{z^2})^1$ orbital. Applying a simple picture of linear combination of atomic orbitals (LCAO) per formula unit, the interaction of three Co-3d orbitals in $Sn_2Co_3S_2$, i.e., triangles of the layers, results in three states: bonging, nonbonding, and anti-bonding. In a simple chemical view, the prominent bands 23, 24, and 25 correspond to these states from 3d interactions in the kagomé-nets as shown in Figure 3b. Accordingly, band no. 23 is fully
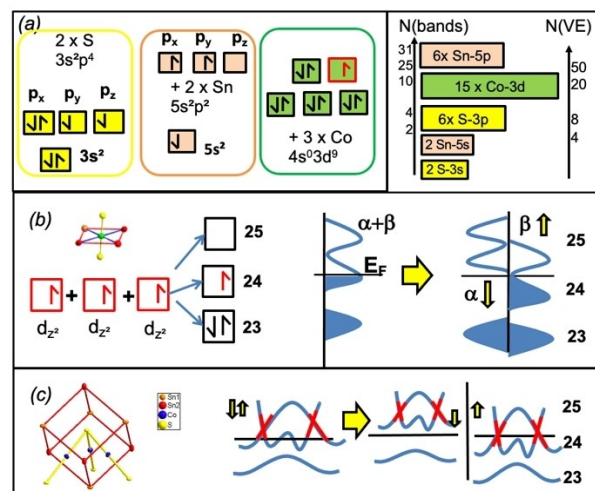

Figure 2. EoS-evaluation of the substitution series $M_3A_2S_2$ (non-spin polarization calculations with PBE-D3).

Legend:
- $Co_3Sn_2S_2$
- $Co_2NiInSnS_2$
- $Co_2NiSnInS_2$
- $CoNi_2In_2S_2$
- $FeNi_2SnIn_2S_2$
- $Fe_2CoIn_2S_2$
- Co_2InSbS_2
- Co_3SbInS_2
- $FeCo_2SbSnS_2$
- $FeCo_2SnSbS_2$
- $Ni_2CoInSnS_2$

Figure 3. Scheme of the electronic structure of $Sn_2Co_3S_2$ with (a) LCAO scheme for the states of the atomic orbitals, (b) interaction of Co-3d orbitals in the valence band region, (c) bands in non-polarized and spin polarized state.
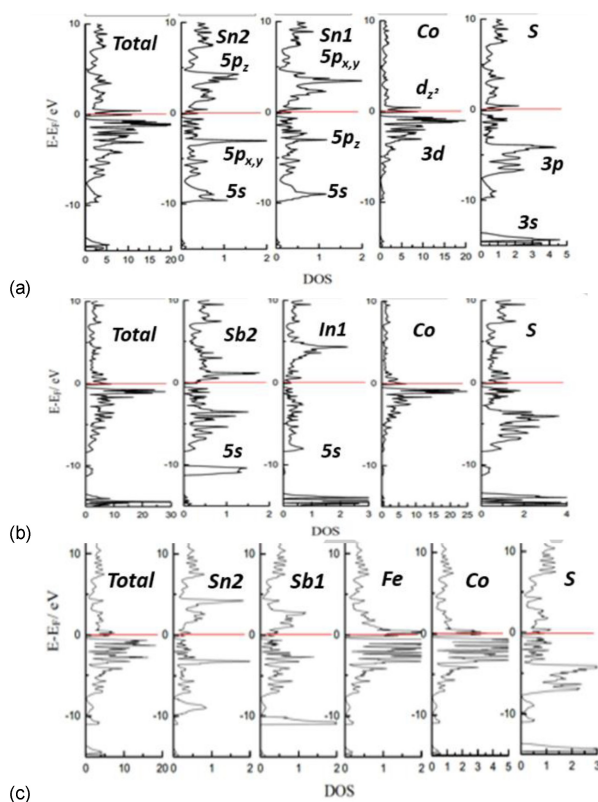
Figure 4. DOS plots for (a) $Sn_2Co_3S_2$, (b) $InSbCo_3S_2$, (c) $SnSbFeCo_2S_2$.

From respective DOS plots for $InSbCo_3S_2$ and $SnSbFeCo_2S_2$ (Figure 4) one can study effects of the substituting atoms. For $A = In$ the 5s and 5p states are shift to higher, for $A = Sb$ to lower energy. In case of $M = Fe$ higher contributions to antibonding states at and above E_F are found in comparison to Co. However, main characteristics of these bands including the Stoner instability at E_F are maintained upon substitution. The compounds might be good candidates for interesting properties.

In Figure 5 specific effects on the electronic structures are analyzed with respect to the topology of their valence bands. The aim is to identify changes in the valence band region with respect to $Sn_2Co_3S_2$ for the design of possible future HFM or topological materials. The band structure of the parent compound $Sn_2Co_3S_2$ is presented in Figure 5a with the prominent topology including Weyl points.[7] The dotted lines signal
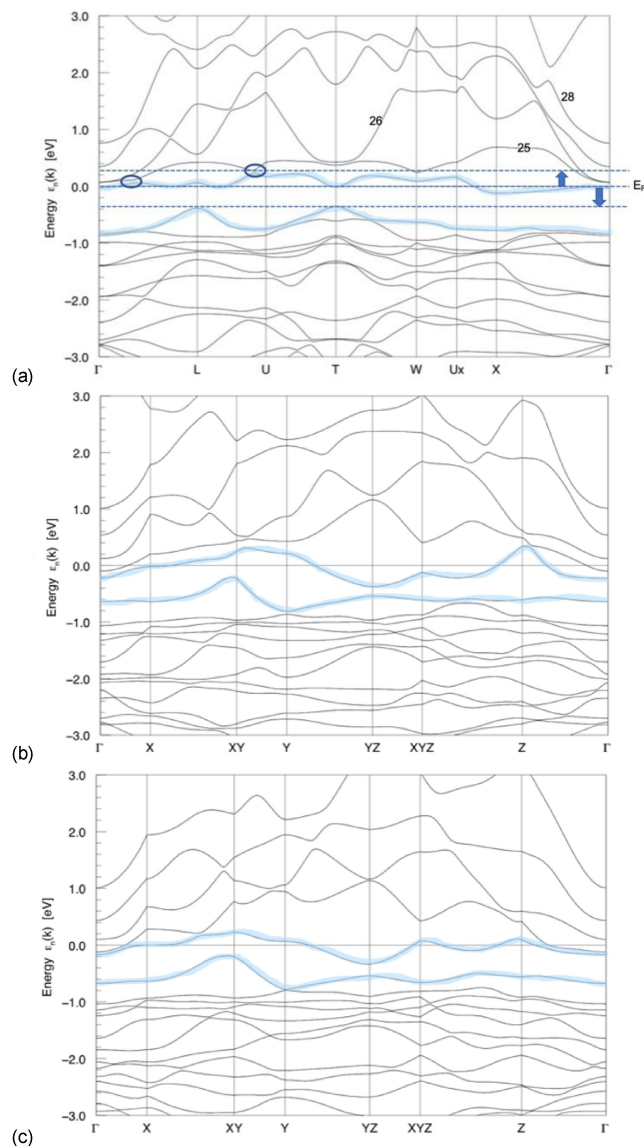
occupied, band no. 24 by only one electron per formula unit. This results in $44 + 2 + 1 = 47$ valence electrons. In the non-magnetic regime this results in the metallic state with half occupied band no. 24. In the ferromagnetic state of $Sn_2Co_3S_2$ band 24 becomes empty for the minority state (down), but fully occupied for the majority spin direction (up). As found by the recent discoveries on topological properties, band 24 and 25 cross at two so called Weyl points that are found at E_F for the majority spin direction, whereas E_F is in the gap between band no. 23 and 24 for the minority spin direction. The respective scheme in Figure 3c signals the unique half metal ferromagnetic and Weyl semimetal state in $Sn_2Co_3S_2$.

Respective atomic site projected density of states is compared in Figure 4 for $Sn_2Co_3S_2$, In/Sb- and Fe substitution. S-3s bands are found at -15 eV, Sn-5s at -8 to -10 eV, followed by S-3p from -3 to -8 eV. Sn-5p states are fond in a wide range from $+5$ eV to -8 eV. Therein, Sn1 and Sn2 differ in degenerate $p_{x,y}$ and p_z contributions. The Co-3d states show main contributions to DOS states between $+2$ and -4 eV with main contributions below and minor above E_F. Just below the Fermi energy the prominent pseudo gap is found. States below represent the occupied 23 bands. Band no. 24 is represented by a DOS maximum at E_F, band no. 25 by a further maximum. Interestingly, orbitals of all atoms contribute to the respective DOS maxima. A simple interpretation was given by interactions in the tetragonal bipyramid coordination of the Co atoms, i.e., CoS_2Sn_4 in the structure of $Sn_2Co_3S_2$ (see HAP scheme).

Figure 5. Electronic band structures of the substitutions series $A_2M_3S_2$ (a) $Sn_2Co_3S_2$, (b) $InSbCo_3S_2$, (c) $SbInCo_3S_2$ in trigonal setting.

the range of the shift of EF for the minority and majority spin directions in the magnetic state. The prominent bands no. 23, 24 and 25 determine the HFM characteristics and the Weyl points. Bands no. 23 and 24 define the pseudo gap formed between them. In case of semiconducting $InSnCo_3S_2$ E_F is found in this gap. In Figure 5 and 6 respective bands 23 and 24 were marked in light blue. In $Co_3Sn_2S_2$ the additional electron, that causes its magnetism, is found in band no. 24. Contacts to band no. 25 determine the prominent Weyl points along Γ-L-U. A simple comparison can be drawn to the modeled structure of $InSbCo_3S_2$. For the first model, i.e., with $A1 =$ In between and $A2 =$ Sb in the Co layers, the obtained band structure is very similar to $Sn_2Co_3S_2$. The pseudo gap is clearly stablished and bands 24 and 25 cross at several points. This situation should become interesting for the search for Weyl points and their modification in future studies. Similar to $SnInCo_3S_2$ a closing of the pseudo gap is seen for $SbInCo_3S_2$ i.e. for $A2 =$ In, $A1 =$ Sb that is attributed to multi-center bonds from analysis of the electron localization function ELF.[18,19,37,38]

Band structures calculated from monoclinic models are compared to $Sn_2Co_3S_2$ in monoclinic setting from Figure 6a. The band structures of $InSnCo_2NiS_2$ (c) and $SnInCo_2NiS_2$ (d) obey the rigid band behavior to first approximation as seen by comparison to $Sn_2Co_3S_2$. The principal scheme of the bands is maintained. However, the topology of the band's changes upon substitution of Co by Ni and Sn by In atoms and leads to a

diminished pseudo gap and increased band dispersion. Contacts of band 24 and 25 that may cause the Weyl points in $Sn_2Co_3S_2$ are modified. For $In_2Ni_3S_2$. $In_2CoNi_2S_2$ does not show a recognizable electronic gap between the two bands. Additionally, both bands cross the fermi level. Therefore, this compound indicates pure metallic properties. With increasing In content half metal states might not be obtained upon spin polarization.

Less expressed differences upon $A1$, $A2$ site occupation are seen for $InSnFeNi_2S_2$ and $SnInFeNi_2S_2$ pictured in Figure 6 g, h.

The band structures of $SbSnFeCo_2S_2$ and $SnSbFeCo_2S_2$ (Figure 6 (i) and (j)) do not show large differences in the band structure upon Sn–Sb ordering. Here, the pseudo gap is clearly expressed, and the compounds might be good candidates for HFM materials.

As seen best for $InSbCo_3S_2$, the mentioned models are good candidate with respect to possible HFM behavior and variation of band topology. The substitutions indicate ways to modify the topology of the band structures and the magnetism of $Sn_2Co_3Sn_2$ and to find novel interesting properties. However, the mentioned properties must be probed by spin polarized calculations with spin-orbit coupling (SOC) in subsequent studies and by experiment.

Conclusion

Starting from shandite type anisotropic $S = \frac{1}{2}$ half metal ferromagnet and Weyl semimetal $Sn_2Co_3S_2 = Co_3Sn_2S_2$ isoelectronic model compounds were investigated by DFT calculations. From electron counting of 47 valence electrons chemical compositions $AA'MM'_2S_2$ were chosen. Balance of the number of electrons was ensured by choice of $A =$ In, Sn, Sb and $M =$ Fe, Co, Ni. Model structures were obtained by partial substitution of the metal A and M sites in low symmetry cells. Thereby, hitherto unknown compositions including $A =$ Sb and $M =$ Fe were considered. According to full structure optimizations within DFT calculations the substitutions allow to alter the cell volume within 10% range compared to $Co_3Sn_2S_2 = Sn_2Co_3S_2$ Structure distortions in terms of interlayer and intralayer atomic distances are shown to depend on compositions atomic site preference. For all compositions specific effects on the electronic structures are found, especially on the three bands that determine half metal and topological features of $Sn_2Co_3S_2$. According to electronic structures several compositions are identified as targets for future experimental and theoretical investigations on magnetic and topological properties. The modeled structures are considered as helpful approximants to study experimental data and to discover novel fascinating multinary shandites as seen for $Sn_2Co_3S_2$ during the last 20 years.

Figure 6. Calculated band structures for (a) $Sn_2Co_3S_2$ (*C2/m* cell), (b) $In_2CoNi_2S_2$, (c) $InSnCo_2NiS_2$, (d) $SnInCo_2NiS_2$, (e) $SnInFeNi_2S_2$, (f) $InSnFeNi_2S_2$, (g) $SbSnFeCo_2S_2$, (h) $SnSbFeCo_2S_2$.

Experimental Section

Calculations of the full structural optimizations and the Equations of State (EoS) were performed by using an LCGTF (linear combination of Gaussian type functions) scheme, which is implemented in the Crystal17 code.[40,41] In the structural optimiza-
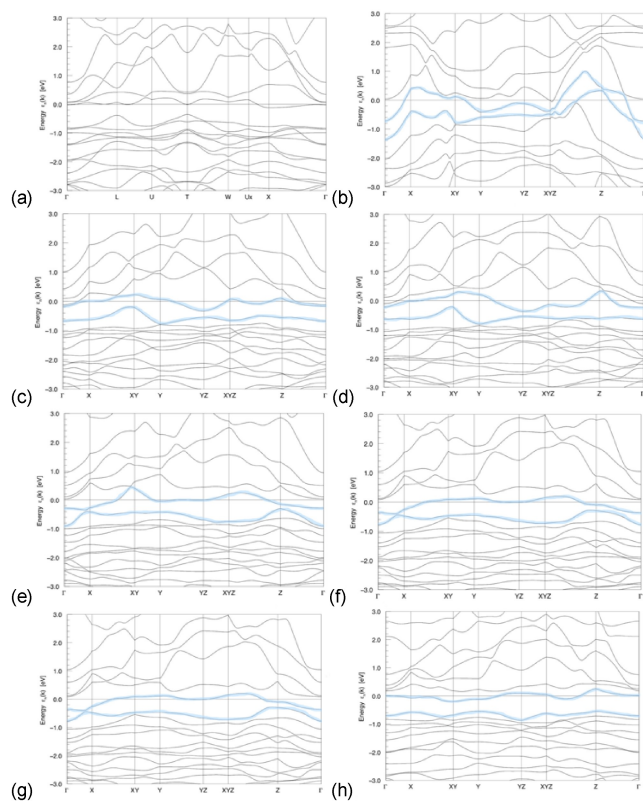
tion as in the calculations of the EOS, the energy considering convergence criteria was set to 10^{-8} H. All DFT studies for structural optimizations started with the parameters a $= 9.331$ Å, b $= 5.403$ Å, c $= 5.458$ Å and $\gamma = 124.55°$. The EOS calculations correspond to ones of Birch-Murnaghan. For Co, Sn, S, Fe, In, Ni, Sb full electron basis sets were used.[42,43]

All calculations of this work were performed with the GGA functional according to Perdew-Burke- Ernzerhoff (PBE) and its extension by Grimme (PBE-D3).[44,45] Convergence criteria were partly varied and amounted to 10^{-6} or 10^{-8}. These are indicated in the input of a calculation, with the keyword TOLDEE. As SHRINK factor (4 8), (6 12) or (12 24) were used. This gives the number of k-points considered. In the spin-polarized calculations, a SPINLOCK was also used starting with (1 7) up to (1 60) was used. For both the geometry optimizations and the EOS calculations, a SPINLOCK was used for the case that in case they did not converge, a MAXCYCLE of 100 was inserted as needed. Additionally, or alone in the same case, TOLDEE of 6 or 8 was inserted. The band structures and the DOS structures were calculated with FPLO.[46]

Acknowledgements

Conflict of Interest

The authors declare no conflict of interest.

[1] P. Ramdohr, *Sitzungsberichte der Deustchen Akademie der Wissenschaften zu Berlin (Mathematisch-naturwissenschaftliche Klasse, Jahrgang 1949)*. **1950**, *6*, 425–439.

[2] M. A. Peacock, Joh. McAndrew, *Am. Mineralog.* **1950**, *35*, 425–439.

[3] J. E. Hiller, *N. Jahrb. Mineral.* **1951**, *12*, 265–277.

[4] A. Michelet, G. Collin, O. Gorochov, *J. Less-Common Met.* **1984**, *97*, 73.

[5] S. Natarajan, G. V. Subba Rap, R. Baskaran, T. S. Radhakarishnan, *J. Less-Common Met.* **1988**, *138.2*, 215–224.

[6] M. Zabel, S. Wandinger, K.-J. Range, *Z. Naturforsch.* **1979**, *34b*, 238.

[7] R. Weihrich, PhD Thesis, University of Regensburg, **2001**.

[8] R. Weihrich, I. Anusca, *Z. Anorg. Allg. Chem.* **2006**, *632*, 1531–1537.

[9] R. Weihrich, R. Pöttgen, F. Pielnhofer, *Angew. Chem. Int. Ed.* **2018**, *57*, 15642–15644; *Angew. Chem.* **2018**, *130*, 15868–15870.

[10] R. Weihrich, I. Anusca, M. Zabel, *Z. Anorg. Allg. Chem.* **2005**, *631*, 1463–1470.

[11] R. Weihrich, S. F. Matar, V. Eyert, F. Rau, M. Zabel, M. Andratschke, I. Anusca, Th. Bernert, *Prog. Solid State Chem.* **2007**, *35*, 309–20.

[12] R. Weihrich, K. Köhler, F. Pielnhofer, Sebastian Haumann, From 3D intermetallic antiperovskites to 2D Half antiperovskites. *Encyclopedia of Inorganic and Bioinorganic Chemistry*, **2017**, DOI: 10.1002/9781119951438.eibc2498.

[13] T. Kubodera, H. Okabe, Y. Kamihara, M. Matoba, *Phys. B* **2006**, *378*, 1142.

[14] W. Schnelle, A. Leithe-Jasper, H. Rosner, F. M. Schappacher, R. Pöttgen, F. Pielnhofer, R. Weihrich, *Phys. Rev. B* **2013**, *88*, 144404–12.

[15] M. Holder, Yu. S. Dedkov, A. Kade, H. Rosner, W. Schnelle, A. Leithe-Jasper, R. Weihrich, S. L. Molodtsov, *Phys. Rev.* **2009**, *B 79*, 205116–9.

[16] X. Lin, S. Bud'ko, P. C. Canfield, *Phil. Mag.* **2012**, *92*, 2436.

[17] A. Umetani, E. Nagoshi, T. Kubodera, M. Matoba, *Phys.* **2008**, *B 403*, 1356.

[18] J. Rothballer, F. Bachhuber, S. M. Rommel, T. Söhnel, R. Weihrich, *RSC Adv.* 2014, 4, 42183–42189.

[19] F. Pielnhofer, J. Rothballer, P. Peter, W. Yan, F. Bachhuber, R. Weihrich, *Z. Anorg. Allg. Chem.* **2014**, *640*, 286–294J.

[20] J. Corps, P. Vaquiero, A. Aziz, R. Grau-Crespo, W. Kockelmann, J. C. Jumas, A. V. Powell, *Chem. Mater.* **2015**, *27*, 3946–3956.

[21] M. A. Kassem, Y. Tabata, T. Waki, H. Nakamura, *J. Crystal Growth* **2015**, *426*, 208.

[22] P. Gütlich, K.-J. Range, C. Felser, C. Schultz-Munzenberg, W. Tremel, D. Walcher, M. Waldeck, *Angew. Chem. Int. Ed.* **1999**, *38*, 2381.

[23] F. Pielnhofer, A. S. Tragl, J. Rothballer, *Z. Naturforsch.* **2014**, *69*, 55–61.

[24] M. A. Kassem, Y. Tabata, T. Waki, H. Nakamura, *J. Solid State Chem.* **2016**, *233*, 8.

[25] M. A. Kassem, Y. Tabata, T. Waki, H. Nakamura, *Phys. Rev.* **2017**, *B 96*, 014429.

[26] D. F. Liu, A. J. Liang, E. K. Liu, Q. N. Xu, Y. W. Li, C. Chen, D. Pei, W. J. Shi, S. K. Mo, P. Dudin, T. Kim, C. Cacho, G. Li, Y. Sun, L. X. Yang, Z. K. Liu, S. S. P. Parkin, C. Felser, Y. L. Chen, *Science* **2019**, *365*, 1282–1285.

[27] E. Liu, Y. Sun, N. Kumar, L. Muechler, A. Sun, L. Jiao, S.-Y. Yang, D. Liu, A. Liang, Q. Xu, J. Kroder, V. Süß, H. Borrmann, Ch. Shekhar, Z. Wang, C. Xi, W. Wang, W. Schnelle, S. Wirth, Y. Chen, S. T. B. Goennenwein, C. Felser, *Nat. Phys.* **2018**, *14*, 1125.

[28] H. C. Wu, P. J. Sun, D. J. Hsieh, H. J. Chen, K. D. Chandrasekhar, L. Z. Deng, C. W. Chu, H. D. Yang, *Mater. Today Phys.* **2020**, *12*, 100189.

[29] A. Ali, S. Shama, Y. Singh, *J. Appl. Phys.* **2019**, *126*, 155107.

[30] M. A. Kassem, A. Tabata, T. Waki, H. Nakamura, *J. Phys. Condens. Matter* **2021**, *33*, 015801.

[31] K. Geishendorf, R. Schlitz, P. Vir, C. Shekhar, C. Felser, K. Nielsch, S. T. B. Goennenwein, A. Thomas, *Appl. Phys. Lett.* **2019**, *114*, 092403.

[32] C. Liu, C. Yi, X. Y. Wang, J. L. Shen, T. Xie, L. Yang, T. Fennel, U. Stuhr, S. L. Li, H. M. Weng, Y. G. Shi, E. Liu, H. Q. Luo, *Science China Phys.* **2021**, *64*, 257511., .

[33] Y. Araki, J. Watanabe, K. Nomura, *J. Phys. Soc. Japan* **2021**, *90*, 094702.

[34] S. Howlader, R. Ramachandran, Y. Singh, G. Sheet, *J. Phys. Condens. Matter* **2020**, *33.5*, 075801.

[35] V. Meschke, P. Gorai, V. Stevanović, E. S. Toberer, *Chem. Mater.* **2021**, *33*, 4373-4381. .

[36] R. Weihrich, W. Yan, J. Rothballer, Ph. Peter, S. M. Rommel, S. Haumann, F. Winter, Ch. Schwickert, R. Pöttgen, *Dalton Trans.* **2015**, *44*, 15855–15864.

[37] I. Anusca, A. Schmid, P. Peter, J. Rothballer, *Z. Anorg. Chem.* **2009**, *635*, 2410–2428.

[38] G. S. Thakur, P. G. Vir, Praveen, S. N. Guin, Ch. Shekhar, R. Weihrich, Y. Sun, N. Kumar, F. Felser, *Chem. Mater.* **2020**, *32*, 1612–1617.

[39] S. M. Rommel, A. Krach, P. Peter, R. Weihrich, *Chem. Eur. J.* **2016**, *22*, 6333–6339.

[40] R. Dovesi, A. Erba, R. Orlando, C. M. Zicovich-Wilson, B. Civalleri, L. Maschio, M. Rerat, S. Casassa, J. Baima, S. Salustro, B. Kirtman, *WIREs Comput. Mol. Sci.* **2018**, *8*, e1360.

[41] R. Dovesi, V. R. Saunders, C. Roetti, R. Orlando, C. M. Zicovich-Wilson, F. Pascale, B. Civalleri, K. Doll, N. M. Harrison, I. J. Bush, P. D'Arco, M. Llunell, M. Causà, Y. Noël, L. Maschio, A. Erba, M. Rerat, S. Casassa, CRYSTAL17 User's Manual (University of Torino, Torino, **2017**).

[42] „CRYSTAL – Theoretical Chemistry Group, „CRYSTAL- A computational tool for solid state chemistry and physics, "Basis sets," **2018**. [Online]. Available: http://www.crystal.unito.it/Basis_Sets/cobalt.html.

[43] M. Towler, „CRYSTAL Ressource Page," **2018**. [Online]. Available: http://www.tcm.phy.cam.ac.uk/~mdt26/basis_sets/.

[44] S. Grimme, A. Hansen, J. G. Brandenburg, C. Bannwarth, *Chem. Rev.* **2016**, *116*, 5105–5154.

[45] S. Grimme, S. Ehrlich, L. Goerigk, *J. Comb. Chem.* **2011**, *32*, 1456.

[46] I. Opahle, K. Koepernik, H. Eschrig, *Phys. Rev. B* **1999**, *60*, 14035.